Towards understanding time-lapse electrical resistivity signals measured during contaminated snowmelt infiltration

Esther Bloem, Nicolas Forquet, Astri Søiland, Andrew Binley, Helen French

Towards understanding time-lapse electrical resistivity signals measured during contaminated snowmelt infiltration

Esther Bloem[1]*, Nicolas Forquet[2], Astri Søiland[3], Andrew Binley[4] and Helen K. French[1,3]

[1]*Norwegian Institute of Bioeconomy Research (NIBIO), P.O. Box 115, Ås, NO-1431, Norway,* [2]*UR REVERSAAL, INRAE 5 rue de la Doua – CS70077, Villeurbanne, 69626, France,* [3]*The Norwegian University of Life Sciences (NMBU), P.O. Box 5003, Ås, 1432, Norway, and* [4]*Lancaster Environment Centre, Lancaster University, Lancaster, LA14YQ, UK*

ABSTRACT

To improve risk assessment, control and treatment strategies of contaminated sites, we require accurate methods for monitoring solute transport and infiltration in the unsaturated zone. Highly spatio-temporal heterogeneous infiltration during snowmelt increases the risk of contaminating the groundwater in areas where de-icing chemicals are required for winter maintenance of roads and runways. The objective of this study is to quantify how the different processes occurring during snowmelt infiltration of contaminated meltwater affect bulk electrical resistivity. Field experiments conducted at Moreppen experimental lysimeter trench are combined with heterogeneous unsaturated soil modelling. The experimental site is located next to Oslo airport, Gardermoen, Norway, where large amounts of de-icing chemicals are used to remove snow and ice every winter. Bromide, an inactive tracer, and the de-icing chemical propylene glycol were applied to the snow cover prior to the onset of snowmelt, and their percolation through the unsaturated zone was monitored with water sampling from 37 suction cups. At the same time, cross-borehole time-lapse electrical resistivity measurements were recorded along with measurements of soil water tension and temperature. Images of two-dimensional (2D) bulk resistivity profiles were determined and were temperature corrected, to compensate for the change in soil temperature throughout the melting period. By using fitted parameters of petrophysical relations for the Moreppen soil, the tensiometer data gave insight into the contribution of water saturation on the changes in bulk resistivity, while water samples provided the contribution to the bulk resistivity from salt concentrations. The experimental data were compared with numerical simulation of the same experimental conditions in a heterogeneous unsaturated soil and used to quantify the uncertainty caused by the non-consistent resolutions of the different methods, and to increase our understanding of the resistivity signal measured with time-lapse electrical resistivity tomography. The work clearly illustrates the importance of ground truthing in multiple locations to obtain an accurate description of the contaminant transport.

Key words: Electrical resistivity tomography, Groundwater, Hydrogeology, Hydrogeophysics, Water saturation.

INTRODUCTION

Our research aims to tackle the challenge of monitoring contaminant transport in the unsaturated zone during snowmelt

*E-mail: Esther.Bloem@nibio.no

infiltration to improve risk assessment, monitoring and treatment strategies of contaminated sites in cold climates. Use of geophysical techniques to monitor hydrogeological (hydrogeophysics) and biological processes (biogeophysics) at the field scale has become widespread (Hubbard and Rubin, 2000; Vereecken *et al.*, 2006; Binley *et al.*, 2015). These techniques can provide physical properties of larger subsurface volumes than traditional soil and soil water sampling techniques and can be more cost-effective. Also, invasive methods are more labour intensive than non-invasive geophysical approaches, and in some cases not possible due to practical limitations. Therefore, it is desirable to reduce the need for invasive surveys, while still being able to explain the ongoing processes.

Time-lapse electrical resistivity tomography (ERT) can be used to characterize solute plume movement and changes in water saturation in the unsaturated zone (French *et al.*, 2002; French and Binley, 2004; Cassiani *et al.*, 2006; Kemna *et al.*, 2006; Chambers *et al.*, 2014; Uhlemann *et al.*, 2017). Changes affecting the bulk electrical resistivity during a snowmelt event include soil temperature, water saturation and electrical conductivity of the pore water and must be assessed separately. The temperature effect can be easily calculated, for example using the approaches suggested by Hayley *et al.* (2007), Chambers *et al.* (2014) and Uhlemann *et al.* (2017), while Archie's law (Archie, 1942; Lesmes and Friedman, 2005) relates water saturation, EC of the pore fluid to bulk electrical resistivity, assuming minimal contribution from surface conductivity.

The study area we focus on is Oslo airport, Gardermoen, Norway, where large amounts of de-icing chemicals are used to remove snow and ice on airplanes (propylene glycol, PG) and runways (potassium formate, KFo) every winter. During snowmelt these chemicals infiltrate along the runway. Although the chemicals are degradable, they might reach the groundwater if degradation rates are not sufficient relative to the pore water velocities in the unsaturated zone. According to the pollution regulations set by the local authorities, the de-icing chemicals should not reach the groundwater and the groundwater chemistry should remain unaffected. A major challenge for airport management is therefore to have sufficient control of contaminant transport and degradation. Currently, only the saturated zone is being monitored, mostly by manually sampling groundwater wells along the runway, providing a limited set of point measurements. Since the subsurface is highly heterogeneous, there is still a challenge to understand the spatio-temporal development of de-icing chemicals over large volumes. Attempts to monitor the unsaturated zone

with suction cups have failed due to clogging of filters caused by high microbial activity, and the physical access to the 70 m security zone along the runway is highly limited, hence new approaches are required (Øvstedal, pers. comm.).

In the present study, we examine how a combination of non-invasive time-lapse electrical resistivity measurements, heterogeneous unsaturated zone modelling and invasive methods (such as soil water sampling with suction cups, tensiometer and soil temperature measurements) can help distinguish between the different contributions to changes in bulk electrical resistivity and explore the pitfalls of only applying one, or a limited number, of methods to monitor contaminated snowmelt infiltration. The underlying hypothesis is that by quantifying the contribution of water saturation, temperature and pore water electrical conductivity to bulk electrical resistivity (that is inferred from ERT measurements), an optimized monitoring method without labour-intensive and disruptive soil water sampling can be proposed. We also explore how unsaturated zone flow and transport modelling can contribute to the interpretation of time-lapse ERT.

MATERIALS AND METHODS

Fieldwork was carried out at the Moreppen field research station, which is dedicated to studies of solute transport in the unsaturated zone. The 2.5 m deep, 3.5 m wide and 7.5 m long trench includes horizontally installed suction cups, tensiometers, soil temperature sensors and vertical boreholes for cross-borehole electrical resistivity measurements (Fig. 1). Moreppen is situated at Oslo airport, Gardermoen, 40 km north of Oslo, Norway (French *et al.*, 1994). The underlying Gardermoen aquifer is the largest rain-fed unconfined aquifer in Norway. The area is a glacial contact delta with sand and gravels dominating near the ground surface underlain by silty glaciomarine deposits (Jørgensen and Østmo, 1990; Tuttle, 1997). The unsaturated zone (1–30 m thick) is heterogeneous, with sediments of fine to coarse sand and gravel. The top set unit is approximately 2 m thick and has horizontal beds of coarse sediments, gravel, gravely sand and medium to coarse sand (Fig. 1). The underlying foreset beds are dipping and contain finer sediments, dominated by medium to fine sand. The top soil at the research station Moreppen does not contain clay, and adsorbed water is therefore not an issue.

The annual precipitation is approximately 800 mm, and the evapotranspiration is about 400 mm. At the research station, the groundwater level is at about 5 m depth. During the snowmelt period (usually of duration 3–5 weeks), more
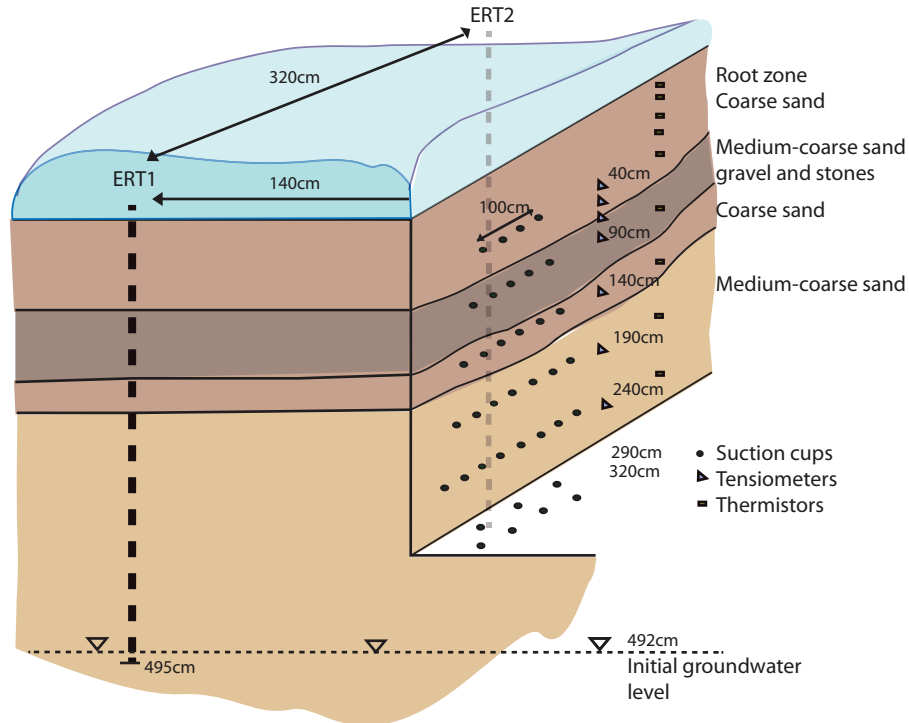
Figure 1 Schematic diagram of the lysimeter trench, including suction cups, tensiometers and boreholes containing electrodes. Temperature sensors (thermistors) are installed on the opposite trench wall, but for simplicity are shown here. De-icing chemical and tracer were added to the snow covering the entire surface area. The distance from the wall to the suction cups increases from 70 cm at the top row to 110 cm at the bottom row, suctions cups below 240 cm depth were tilted to reach larger depths from the trench wall.

than 50% of the groundwater recharge occurs (Jørgensen and Østmo, 1990).

A tracer experiment was performed during the snowmelt period of 2010. The surface of the snow, next to the Moreppen research trench (Fig. 1), was supplied with 1000 g degradable propylene glycol PG/m^2 and 10 g Br/m^2 (from NaBr), as an inactive tracer. This was done on 26 March 2010, Day 00, approximately 6 days before the main snowmelt started. The groundwater table was measured at 4.92 m below ground level. The specifications of the tracer experiment are given in Table 1. During the experiment, snowmelt, precipitation, groundwater levels, soil and air temperatures were monitored.

Table 1 Specifications of the tracer experiment at Moreppen

	South wall
Date of applications	March 26, 2010
Amount of applied de-icing chemicals	1000 g PG/m^2
Commercial name of de-icing chemical	Kilfrost type II
Applied inactive tracer	10 g Br/m^2
Area where chemicals were applied	4.2 × 3 m = 12.6 m^2

Transport of solutes was monitored by cross-borehole electrical resistivity measurements and by taking water samples with suction cups. Soil water suction was monitored with tensiometers.

The snowmelt at Moreppen was monitored by repeated snow core sampling (average snow water equivalent in millimeters of three points on measured dates). The total amount of available water for infiltration during complete snowmelt was then validated with the sum of snow water equivalent at the beginning of the experiment plus the total precipitation measured at the weather station at the Oslo airport during the same period.

Soil temperature, measured with thermistors (Campbell Scientific 107) with an accuracy of 0.1 °C, were logged every hour at depths: 0.05, 0.10, 0.15, 0.20, 0.30, 0.40, 0.90, 1.40, 1.90 and 2.40 m. The thermistors were inserted 100 cm into the trench wall (Fig. 1). Air temperature was also measured on an hourly basis.

A pair of 4.95 m deep boreholes, each with 34 stainless-steel electrodes (0.15 m spaced), separated by 3.2 m, for cross-borehole electrical resistivity tomography (ERT) measurements were installed 1.4 m from the south wall of the

trench (Fig. 1). A Syscal Pro Switch (Iris Instruments) was used to obtain the ERT measurements. The measuring time for each quadrupole was set to 1 s with an injection voltage of 100 V. In-hole and cross-borehole dipole–dipole configurations were used with a fixed dipole spacing of 0.45 m (three electrode-pair spacings) for both the current and potential electrode pairs. One advantage of using a dipole–dipole configuration (with the Syscal Pro Switch) is that the acquisition time is reduced due to the possibility of multi-channel measurements. Data collection of one dataset took approximately 1.5 hours. It is argued by Winship *et al.* (2006) that the data capture time can be critical in time-lapse studies and is recommended to be short as possible since each image should reflect a 'snapshot' of the infiltration through the subsurface. To ensure good data quality, both normal and reciprocal (swapping potential and current electrodes) dipole–dipole measurement were collected, making a total of 4148 measurements. Reciprocity checks are useful for assessing measurement errors and data weights for the inversion process (e.g. Binley, 2015; Tso *et al.*, 2017).

At the south wall of the trench soil water samples were taken from a set of 37 suction cups installed at depths 0.40, 0.90, 1.40, 1.90, 2.40, 2.90 and 3.20 m, during the snowmelt period (Fig. 1). The suction cups (Prenart Equipment) are made of Teflon (Teflon avoids ion sorption compared to using ceramics), have a pore size of 2 μm, and a porous area of 33 cm^2. A vacuum pump ensured the designated constant suction of 0.15 bar of the setup (French *et al.*, 1994). A closed system of PVC pipes connects each suction cup in the soil profile to its respective collecting bottle inside the trench. To compare data gathered with suction cups with tensiometer and ERT data, we averaged the electrical conductivity (EC) in soil water samples per depth to create a one-dimensional (1D) profile. Tensiometers to measure the suction were located at 0.40, 0.56, 0.72, 0.90, 1.40, 1.90 and 2.40 m depths at the south wall of the trench. Readings were automatically taken every 5 minutes.

Data processing

A set of ERT measurements were made each monitoring day. From the normal and reciprocal measurements collected in the field, a measurement error estimate was calculated for each data point by comparing reciprocal and normal measurements. Measurements with a difference between the normal and reciprocal higher than 30% were removed from the dataset. Also, normal or reciprocal data with a repeatability difference higher than 10% were excluded, together with measurements with a geometric factor higher than 10,000.

Data used in the inversions are average values of reciprocal and normal values. The filtering process resulted in 999 measurements common in all datasets. For each dataset, a unique measurement error (E_{data}) model was calculated subdividing resistance values into bins according to their values, creating averages of errors and resistances for each bin and calculating a linear regression equation (Köestel *et al.*, 2008). Although two-dimensional (2D) arrays were used for ERT data collection, it was necessary to model the data in three-dimensional (3D) to account for the nearby trench wall (Fig. 1). For the ERT modelling, an unstructured tetrahedral prism mesh was generated using the software Gmsh (v2.5; Geuzaine & Remacle, 2009). The mesh consists of an 'infinite' half-space (dimension of 66.4 m × 62.8 m × 35.0 m), with a trench void included to account for the effect of the nearby trench. Around the boreholes, two cylinders (0.20 m in diameter, with a meshing characteristic length of 0.05 m) were included in the mesh to minimize the effect of the boreholes in the inversion results. A larger meshing characteristic length was adopted for the boundary of the mesh. The 3D mesh consists of 114,606 elements. The forward modelling error (E_{model}) was estimated for each quadrupole using similar mesh discretization without the trench, thus permitting the computation of an analytical solution. This error was combined with the measurement error to give the combined individual error (*Err*) for each measurement as:

$$Err = \sqrt{\left(E_{\text{data}}^2 + E_{\text{model}}^2\right)}. \tag{1}$$

The inversions of the measured resistivity datasets were done with the code R3t (v2.0; http://www.es.lancs.ac.uk/people/amb/Freeware/R3t/R3t.htm, 2019). Isotropic smoothing was adopted within the inversion. In addition to the inversion of the individual datasets, we also inverted the data with a time-lapse approach using ratio inversions (e.g. Binley, 2015). Here the data are transformed by taking the ratio of transfer resistances collected at later time steps relative to the initial dataset. The dataset can then be inverted to recover relative changes in resistivity.

The resistivity models from individual inversions were corrected for temperature after inversion to be able to quantify changes in electrical resistivity due to changes in soil water content and solute concentration. The electrical resistivity of pore water decreases with temperature due to increase in ion agitation as a result of decreasing viscosity of the fluid, while the change in the surface electrical resistivity of rocks and sediments due to temperature variations are caused by changes in the surface ionic mobility. Rein *et al.* (2004) showed that

even diurnal temperature variations can have a relatively large effect on the electrical resistivity. For the temperature range 0–25°C, the temperature dependency is not well described with petrophysical models (Llera *et al.*, 1990) calibrated to the range 25–200°C. For temperature range 0–25°C, we used the linear approximation suggested by Hayley *et al.* (2007):

$$\sigma_{\text{std}} = \left[\frac{f\,(T_{\text{std}} - 25) + 1}{f\,(T_i - 25) + 1} \right] \sigma_i, \tag{2}$$

where σ_{std} (S/m) is the bulk electrical conductivity at the standard temperature, T_{std} (°C) is the standard temperature, σ_i (S/m) is the *in situ* bulk electrical conductivity, T_i (°C) is the *in situ* temperature and f (1/°C) is the fractional change in bulk electrical resistivity per °C for 25°C. Hayley *et al.* (2007) found f to be 0.0183. As temperature correction experiments have not been carried out before for Moreppen sand, the f suggested by Hayley *et al.* (2007) was used in this work.

The measured soil temperatures during the ERT collection time were used for the temperature correction. The profile was divided into layers based on the intervals between the upper and lower thermistors depths. Due to the lack of deeper thermistors, the temperature measurement at 2.4 m was applied down to 3.5 m. From observations, we know that the deeper layers show less temperature variations due to insulating effects from changes in air temperature. Equation (2) was applied to pixel values of the individual inversions, using 25°C as the standard temperature.

The conversion of soil water suction, measured by tensiometers, to bulk electrical resistivity consists of two steps. The first step is to translate suction to fluid saturation. The second step is to translate fluid saturation to bulk electrical resistivity. For both steps, additional site-specific parameters are needed. These can be derived from laboratory measurements of the water retention curve, which describes the relationship between the water content and soil water potential from soil samples taken at the research site. The van Genuchten model (1980) was used:

$$\theta\,(\psi) = \theta_r + \frac{\theta_s - \theta_r}{\left[1 + (\alpha\,|\psi|)^b \right]^{1-1/b}}, \tag{3}$$

where S is the saturation, ψ is the suction pressure (L), θ_s is the saturated water content (L^3/L^3), θ_r is the residual water content (L^3/L^3), α is related to the inverse of the air entry suction and must be larger than zero (1/L), and b (-) is related to the pore-size distribution.

Defining the effective saturation (S) as

$$S = \frac{\theta\,(\psi) - \theta_r}{\theta_s - \theta_r}. \tag{4}$$

The van Genuchten equation can then be rewritten in terms of effective saturation:

$$S = \frac{1}{\left[1 + (\alpha\,|\psi|)^b \right]^{1-1/b}}. \tag{5}$$

To calculate the saturation from the measured suction, we used: $\theta_s = 0.35$; $\theta_r = 0.078$, $\alpha = 0.02$ 1/cm, and $b = 2$. These van Genuchten parameters are based on a typical water retention curve from the site (Pedersen, 1994; French *et al.*, 2001; Forquet, 2009). The average suction values measured with tensiometers during the same time as the ERT measurements (i.e. a 2-hour period) were used to calculate the contribution to the bulk resistivity.

Many authors have investigated the relationship between water content and bulk electrical resistivity (as presented in the literature review by Lesmes and Friedman, 2005). Some authors (Feng and Sen, 1985; Mualem and Friedman, 1991) suggested conceptual approaches to model this relationship. Forquet (2009) found the more common and easier to adapt empirical model Archie's law (1942), which assumes no surface conductivity, is the most suitable to use for the soil at Moreppen:

$$\rho_{\text{bulk}} = F\rho_w = \frac{1}{\sigma_w}\phi^{-m}S^{-n}, \tag{6}$$

where ρ_{bulk} is the bulk electrical resistivity of the soil, F is the formation factor, ρ_w is the pore fluid electrical resistivity, σ_w is the pore fluid electrical conductivity, ϕ is the porosity, m is the Archie cementation factor, S is the saturation and n is the Archie saturation exponent. In our study, both saturation and pore water electrical conductivity change.

Pore water electrical conductivity was measured in water samples taken with suction cups and saturation, S, inferred from equation (5). For the soil at Moreppen, the best fit of m and n was 1.89 and 2.21, respectively, based on calibration curves using different saturation levels and salt solutions (Forquet, 2009). We assume a porosity of 0.35, which fits well within the measured range of 0.3–0.4 given by Pedersen (1994) and Forquet (2009) and is consistent with previous unsaturated zone simulations from the site (French *et al.*, 2001). Archie's law has been verified down to low saturation levels, especially in fine-textured materials. It has been well-verified for coarse sand which is of relevance for the Moreppen sediments.

To study the contribution of changes in saturation and electrical conductivity to the bulk resistivity, we computed bulk resistivity profiles using the Archie parameters described above. To assess the impact of saturation changes, the bulk

resistivity was computed assuming a constant (pre-tracer) pore water conductivity of 26 μS/cm and the bulk resistivity calculated with the measured changes in saturation. A similar set of calculations to determine the effect of pore water conductivity changes was made using the average saturation value of 0.8 measured over the experimental period, while including observed pore water conductivity. Finally, we used both observed saturation and observed electrical conductivity of the pore water in equation (6) to calculate the bulk resistivity on each measurement day, which can be directly compared to the bulk electrical resistivity from the inversion of ERT data, extracted from the central 1.6 m wide region of the ERT image (since this represents the zone monitored by the suction cups; Fig. 1).

A risk when comparing measured (ground truthed) point data with integrated resistivity values obtained through inversion of the electrical resistivity measurement is that the point measurements do not give a representative value because of the natural heterogeneity of the soil. In order to illustrate the theoretical expectations of changes in water saturation and tracer concentration, we simulated the water flow and solute transport during snowmelt with Hydrus 2D/3D (Šimůnek, *et al.*, 2016) version 3.01, which models the flow and solute transport in partially saturated soils. The simulated soil water profile is consistent with the above description: 4.95 m to the groundwater level (*Z* direction), and van Genuchten parameters (equation 3) as shown above: $\theta_s = 0.35$; $\theta_r = 0.078$; $\alpha = 0.02$ 1/cm and b = 2. The saturated hydraulic conductivity, K_s, was set equal to 5.6×10^{-4} m/s, which is consistent with previous simulations of the same site (French *et al.*, 2001). The heterogeneity of the soil profile was defined by the Miller and Miller similarity (Miller and Miller, 1956), with a standard deviation of $\log_{10} K_s$ equal to 1. The length (*X* direction) of the surface domain was set to 3.2 m, which is the same as the separation between the ERT boreholes. To account for possible 3D effects the width of the model (*Y* direction) was set at 0.5 m. The grid contains 80,572 finite elements, with element size of 3.8 cm in the *X*–*Z* direction and 3.6 cm in the *Y* direction. The top boundary was supplied with a time-variable infiltration rate over 31 days based on the field measurements of daily snowmelt and rainfall (Fig. 2b). The vertical boundaries were considered no-flow boundaries, and atmospheric pressure (groundwater level) was defined at the lower boundary, which was consistent with the observed groundwater level. To account for the water transport to the groundwater zone, a flux of 0.4 cm/d was assigned at the groundwater level. To study the transport process, the equivalent of 2 L/m^2 of tracer solution concentration of 0.0625 mol/L was supplied as a

pulse to the surface boundary with the infiltrating water on day 2 (i.e., 10 g Br per m^2), the day before the natural melting started. This mimics the real situation where the de-icing chemicals enter the soil with the first meltwater.

RESULTS

The first major melting of the snow cover started on day 6 (April 1) (Fig. 2), this is also a turning point for the groundwater level, which starts to increase from its deepest level of 4.95 m, showing a rapid response of the groundwater level to the snowmelt. During the entire snowmelt period (ending April 16 (day 21)), the groundwater level increases by 0.39 m to a depth of 4.56 m. After this, the groundwater level stabilized. The total release of melt and rainwater during the experiment was measured to be 245 mm.

As snow cover melts and there is no longer an insulation effect against air, soil temperature increases near the surface (Fig. 3). The soil temperature near the surface changed from −0.6 to 4.4°C during the 31 days of the experimental period. This increase in temperature is reduced with depth, with the smallest increase of 0.27°C at 2.4 m depth. As the soil temperatures in the upper 0.4 m were below freezing until day 19 (April 14) while there is no surface ponding, it is assumed that meltwater infiltrated the upper frozen layer (negative soil temperature and presence of ice could be observed mechanically with a spade).

To compensate for increased temperature over time, a temperature correction of the ERT survey data was conducted. This also removed the effect of vertical temperature variability. This is important because we want to compare the bulk resistivity with other measurements, such as EC measurements in collected water samples, which are already temperature corrected. The overall effect of temperature correction is that the resistivity values throughout the profile are reduced (Fig. 3b). We found an average temperature correction factor of 0.56, with the largest change at the surface at 0.05 m depth (with minimum and maximum correction factor of 0.53 and 0.62) and lowest at 2.4 m depth (variation of 0.005 between minimum and maximum). As can be seen in Fig. 3(b), the temperature corrections during our study period caused a nearly constant shift.

Figure 4 shows the inversions of individual ERT datasets, extracted within the region between the two boreholes. The high resistivity above the water table is consistent with well-drained coarse sediments combined with low electrical conductivity of native pore water. The images are also consistent with the 2D ERT inversions reported by French
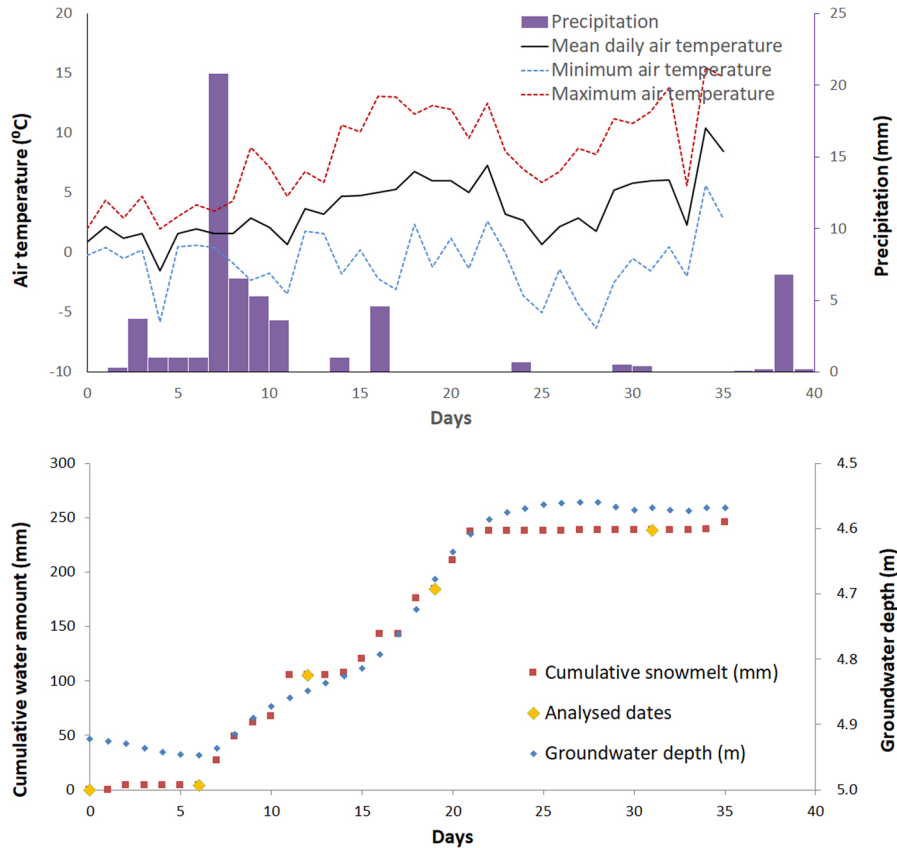
Figure 2 Mean, minimum and maximum daily air temperatures and precipitation (a) and cumulative snowmelt (corrected for precipitation) and groundwater level below surface (m) (b) during snowmelt period (March 26 to April 30, 2010) at Moreppen. The analysed dates are indicated with yellow points.

et al. (2002) for a different borehole pair used for an earlier experiment at the same field site.

The individual inversions (Fig. 4) show reduced resistivities until day 19; on day 31, resistivities increased slightly but did not return to the initial state. The ratio (time-lapse) inversions (Fig. 5) reveal the changes in resistivity much clearer. A gradual downward movement of low resistivity consistent with infiltration can be seen. From Figs 4 and 5 alone it is difficult to decipher how much of the change in bulk electrical resistivity is due to water saturation increase and how much is caused by the solutes (causing an increased electrical conductivity (EC) of the soil water).

Figure 6(a) shows the soil water saturation calculated from the measured suction (tensiometers) along the profile for days 0, 6, 12, 19 and 31. From day 0 to day 6, there is a significant wetting of the upper layer, giving a saturation close to 1 (consistent with the drop in resistivity shown in Figs 4 and 5). On day 12 and 19, further infiltration increases saturation levels to around 0.9 throughout the whole profile.

The soil water samples indicated an electrical conductivity of the snowmelt of around 7 μS/cm, while the background electrical conductivity of the pore water was around 26 μS/cm (average of the profile on day 0). The maximum electrical conductivity of the water samples (155 μS/cm) was measured at 0.40 m depth on day 12 (Fig. 6b). The peak value of electrical conductivity gradually moved downward and reached a maximum at 1.9 m depth on day 31 (Fig. 6b).

The influence of saturation (calculated with equation 6) on the bulk resistivity is only apparent on day 6 in the top meter of soil (Fig. 7), when we observed a soil close to saturation. Here, the bulk resistivity calculated with the observed saturation and background electrical conductivity shows the same trend as the ERT-derived bulk electrical resistivity. Once the whole profile was wetted (on day 12 and 19), that is homogeneous and high saturation, and this is combined with a constant electrical conductivity of the pore water, this gives constant bulk electrical resistivities (Fig. 7). The influence of

Figure 3 Soil temperature profiles measured at Moreppen research station on corresponding days as ERT measurements on day 0, 6, 12, 19 and 31 (a) and the temperature correction factor which has been applied to the modelled electrical resistivity (from the inversion of ERT data) (b).
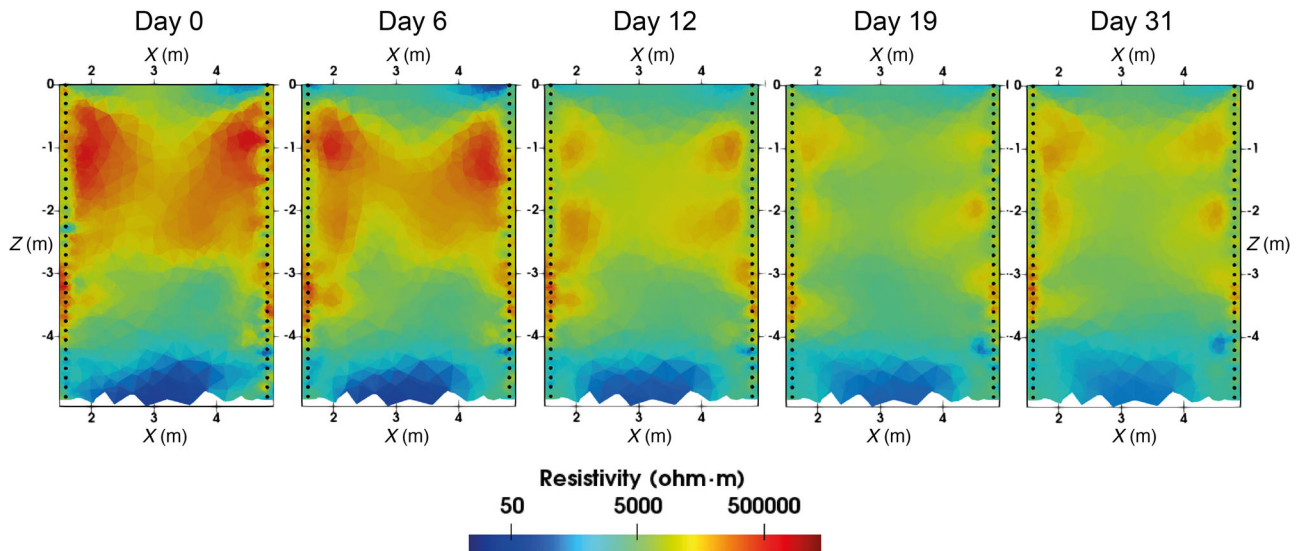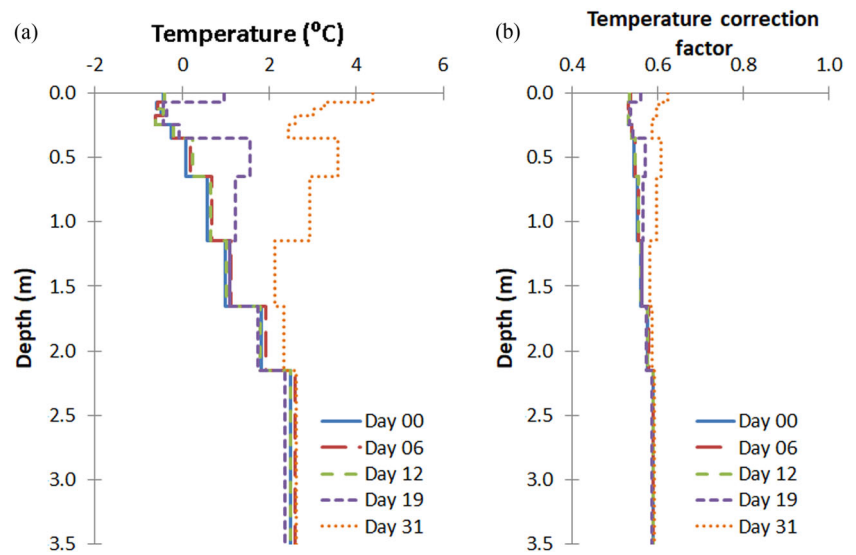

Figure 4 Inversion results of ERT data from day 0, 6, 12, 19 and 31. On the *x*-axis is the distance and on the *z*-axis is the depth.

electrical conductivity of pore water with a constant saturation level (calculated with equation 6), shows little effect on day 6 (the tracer has not yet infiltrated), but strong effect on day 12 and 19 (Fig. 7) when the tracer infiltrates and moves downward.

On day 6, the electrical conductivity of the pore water was roughly constant throughout the measured profile, that is the tracer has not reached the suction cups. The tensiometer near the ground surface shows almost full saturation on the same day, which creates large vertical differences not observed later (Fig. 7). Although the estimated bulk electrical resistiv-

ity (purple stippled line in Fig. 7) does not match exactly the ERT measured bulk electrical resistivity, they are similar. On day 12 and 19, the effect of the fluid resistivity (calculated from pore water electrical conductivity) is clearly visible, as the solutes move downwards from the top and gradually dilutes. The trend, as observed with the combined bulk resistivity, matches well with the interpretation of Figs 4 and 5. During these days, the contribution of the fluid resistivity dominates the combined bulk resistivity. The ERT bulk resistivity shows the same trends, but is smoother than the combined values and shows lower resistivity values (except for day 12)
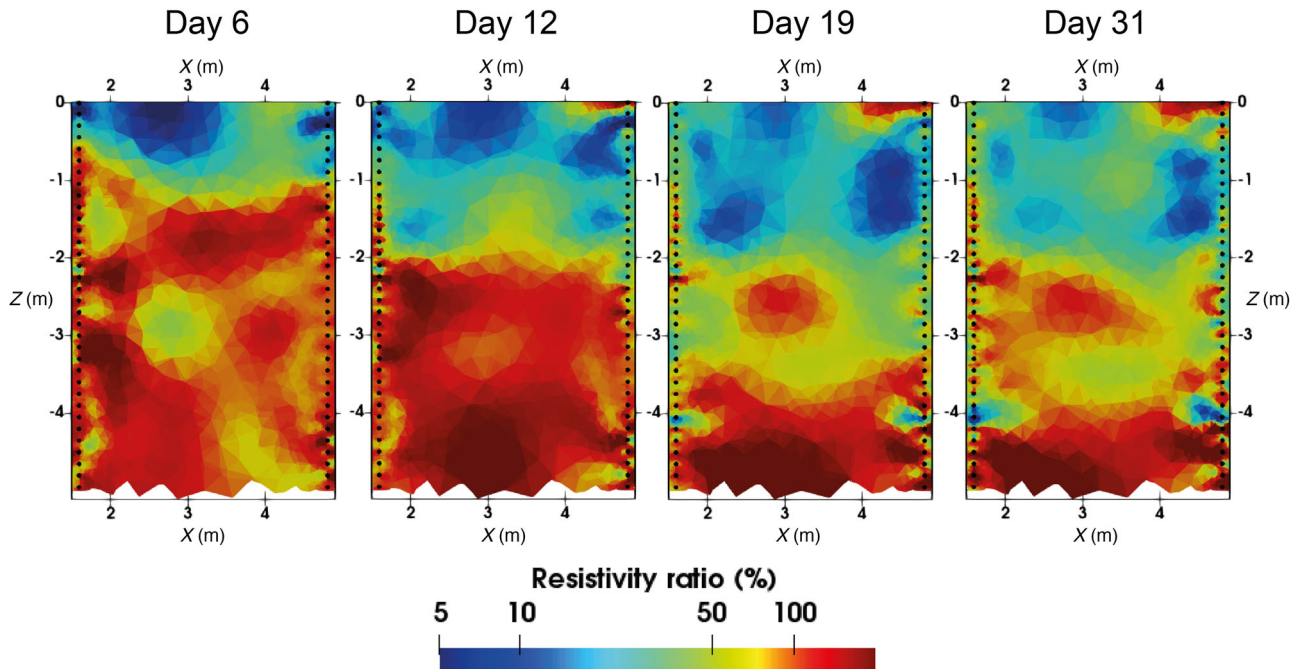
Figure 5 ERT ratio inversion results with background dataset from day 0 on day no. 6, 12, 19 and 31. On the *x*-axis is the distance and on the *z*-axis is the depth.
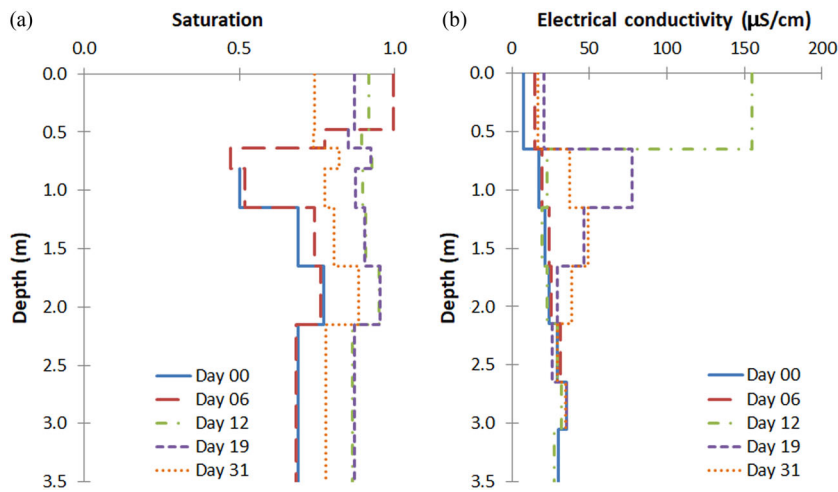

Figure 6 Saturation profiles calculated from the suction measurements (a) using equation (5), and EC profiles of pore water sampled with suction cups on day 0, day 6, day 12, day 19 and day 31 (b).

at the top of the profile and shows higher resistivity values deeper in the profile.

Results of simulations with Hydrus 2D/3D, without any calibration, show an overall flow and transport pattern similar to what is observed with the time-lapse ERT measurements. The saturation profiles (Fig. 8a) indicate only small changes over the 31-day period. Near the surface, average saturation varies between 0.39 and 0.44, while at 3.5 m

depth the average saturation remains close to 0.5, while the variability at this depth increases. Only the upper 3.5 m of the profile is shown to be consistent with the depth of field measurements. The variability of the saturation caused by the modelled heterogeneity is shown by the lower first and third quartiles in Figure 8(a). The minimum and maximum values observed in the simulated profile within these depths range from the residual water content to nearly saturated
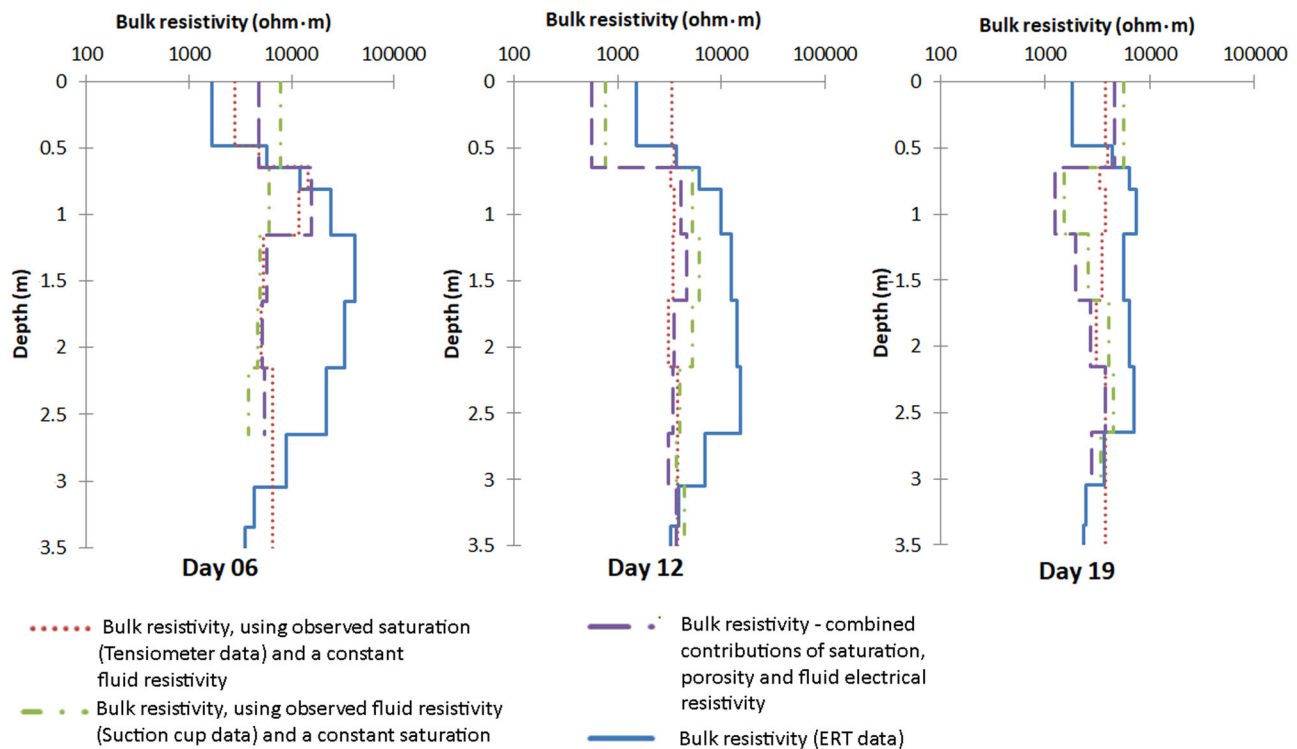
Figure 7 Layer averaged bulk resistivities calculated from temperature corrected ERT inversions (blue lines). Independently estimated combined bulk resistivity (purple stippled line) (equation 6). The bulk resistivity calculated with the observed saturation and constant electrical conductivity background (red lines, tensiometers, equation 6). The bulk resistivity calculated with the observed electrical conductivity of pore water and a constant saturation level (green line, calculated with equation 6).

conditions (saturation = 0.98); this is the case throughout the entire profile. Much larger differences, as might be expected, can be seen in the changes in the fluid electrical conductivity (Fig. 8b). The concentrations given by the simulation were transformed to pore water electrical conductivity by multiplying the concentration of the cation (Na^+) and anion (Br^-) parts (which are assumed to be the same) with their respective molar conductivities (0.05011, 0.0781 S·L/mol·cm) and adding the background conductivity of 25 μS/cm (based on water samples from the suction cups prior to the tracer infiltration). The vertical movement of the zone of elevated pore water electrical conductivity is similar to observations made in the field (EC measured in water from suction cups), though the absolute values are somewhat higher in the observations.

Due to the heterogeneity of the hydraulic conductivity defined in the model, the concentration of tracer spreads in a rather erratic manner, though averaging over horizontal layers will smooth out this effect. The differences in concentration that could potentially be measured by the limited set of suction cups is clear.

DISCUSSION

The snowmelt infiltration at the site can be described by a maximum saturation near the surface reached on day 6 (Fig. 6a), while the maximum pore water electrical conductivity is reached on day 12, indicating a piston-type flow where the old water is replaced by the infiltrating water containing solutes. From previous snowmelting experiments (French and van der Zee, 1999), we know that the de-icing chemicals and tracer will most likely leave the melting snowpack prior to the main infiltration period. This in combination with a heterogeneously distributed ice cover/frozen ground and infiltration pattern (French and Binley, 2004) may give rise to preferential flow paths.

As the water containing solutes reach greater depths, it is diluted because of dispersion. Tensiometer measurements will help distinguish the two effects. In general, we can explain the electrical resistivity tomography (ERT) inversion results (Figs. 4 and 5) and the one-dimensional (1D) transformed profiles (Fig. 7) with the observed changes in saturation
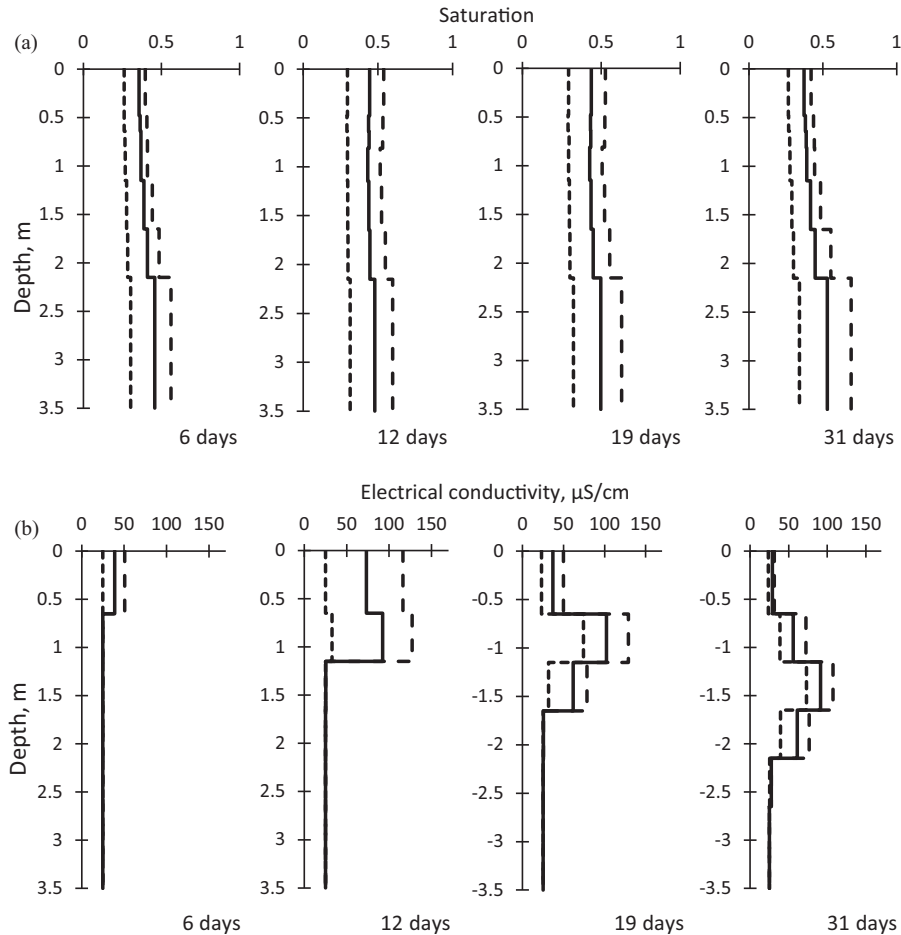
Figure 8 Simulated saturations (a) and EC in the pore water (b), averaged per layer consistent with tensiometer and suction cup depths accordingly, development over time (days 6, 12, 19 and 31). Solid line shows average EC, and stippled lines show upper and lower 25% quartiles.

(calculated from tensiometers) (Fig. 6a) and soil water conductivity measured in water from suction cups (Fig. 6b).

When quantifying the modelled bulk electrical resistivity (from the inversion of ERT data) and the contributions of saturation and pore water electrical conductivity, it is important to include the temperature correction. The temperature corrected bulk resistivity is lower than that observed (temperature correction factor was, on average, 0.56; Fig. 3b). In the observed temperature range, this correction is simply a shift in resistivity values; however, studies from Krautblatter *et al.* (2010) and Wu *et al.* (2017) have shown that below 0 °C the temperature correction factor changes and $f = 0.0183$ 1/°C (equation 2) is not valid. Since our soil temperature does not drop below −0.6°C and occurs only at the top of our profile for a short period, we do consider such a correction. The tracer and de-icing chemicals will reduce the freezing point and will

probably have a local effect, especially at the beginning of the snowmelt infiltration. However, the spatio-temporal variability of this effect is difficult to quantify and the effect will quickly be reduced due to the dilution effect through the transport process. We therefore argue that the *f* parameter for the purpose of this study can be kept constant.

Overall there is a good correspondence between the estimated bulk resistivity calculated from Archie's law from a set of point measurements and the inversion of time-lapse cross-borehole ERT measurements of the same vertical profile. Possibly the discrepancy between the ERT and the combined bulk resistivity profiles (Fig. 7) could be caused by an underrepresentation of the saturation explained by uncertainties in the van Genuchten parameters. The measured water retention parameters (Pedersen, 1994; Forquet, 2009) show great variation which needs to be considered in the
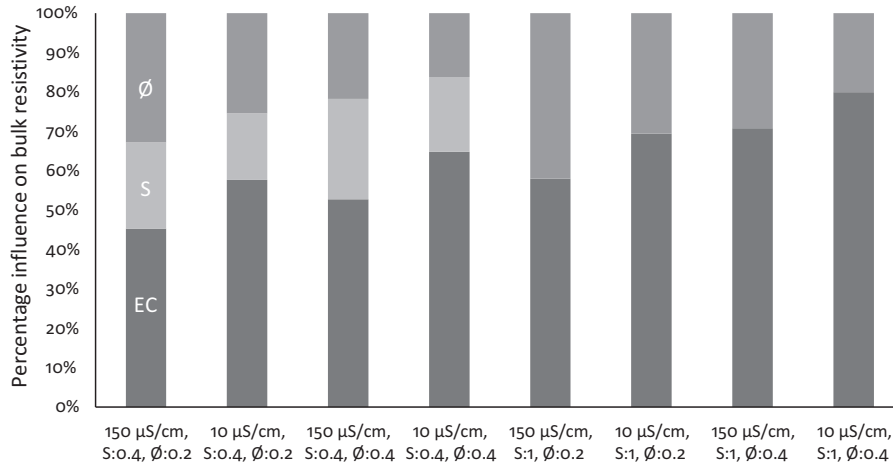
Figure 9 The percentage contribution of EC of the pore water, saturation (*S*) and porosities (Ø) on the normalized (100%) $\log_{10}$ bulk resistivity, when assuming feasible ranges of parameters for the studied field used in equation 6, given along the *x*-axis.

interpretation. In Fig. 9, we have estimated the bulk resistivity (using equation 6) for different combinations of porosity (0.2–0.4; Pedersen, 1994; Forquet, 2009), saturation (0.4–1.0, average from Hydrus modelling and measured values) and electrical conductivity of the pore water (from 10 μS/cm measured in melted snow to 150 μS/cm the highest value measured in pore water). The bulk resistivities have been normalized to 100%, for the sake of comparison. The figure illustrates that under the conditions expected during the snowmelt in this type of soil, the fluid electrical conductivity dominates the bulk resistivity during wet conditions, while the saturation can give similar effects when the soil water conductivity is low (non-contaminated meltwater). This was observed in the field. This conclusion is supported by the sensitivity analysis performed by Forquet (2009, chapter 5). He showed that bulk electrical resistivity was mainly influenced by water content changes, when water contents are low. Above a certain threshold value, bulk electrical resistivity becomes more sensitive to pore water electrical conductivity, while variation in porosity has a negligible effect. It is clear that it is important to quantify at least one of these changes during such a monitoring experiment.

Uncertainty in the *in situ* water contents is also caused by only having one tensiometer per depth, which may not represent the 'true' value. The main difference between the Hydrus simulations and point measurements based on the 1D transformed profiles (Fig. 8) is a lower average saturation in the model than that calculated from tensiometers, and a higher average pore water electrical conductivity in the model compared to what is measured in the water samples. This would cause somewhat different contributions to the bulk

resistivity. Another reason for the discrepancy between the ERT-estimated bulk electrical resistivity profile and the saturation/electrical conductivity (combined) estimated electrical resistivity could be caused by the effect of higher resistivity values closer to the boreholes in comparison to those towards the middle of the profile (the fluid resistivity measurements were taken closer to the middle of the profile).

The snowmelt infiltration is captured well in the numerical simulations without the use of any calibration procedures. Because spatial variability of the hydraulic properties are included, the simulations help to describe the possible ranges of saturation and concentration that could be measured by single point measurements. In a real contaminated site scenario, simulated saturations showing the likely range of saturations could be combined with a limited set of tensiometers at different depths and time-lapse ERT monitoring to indicate the most likely depth range of the contaminants. This would be highly relevant for assessing any remedial actions to be taken.

One of the advantages of the ERT measurements is that changes both in the saturated and unsaturated zones can be monitored, while a combination of suction cups and groundwater wells are required for water sampling. If sensors are installed horizontally from a trench wall, as in this study, the depth of installation is limited to the upper few metres (2.4 m horizontal, and maximum 3.2 m depth slightly at an angle in this study; Fig. 1). Monitoring groundwater levels are also vital for the interpretation, but without the knowledge of residual contaminants that are still present in the unsaturated zone, wrong actions may result.

CONCLUSIONS

With the combination of ERT, tensiometer and suction cup measurements, we were able to observe the differences in snowmelt infiltration and transport of de-icing chemicals in the unsaturated zone. The results show a piston-type flow where the old water is replaced by the infiltrating water containing solutes. As the water containing solutes reaches greater depths, it is diluted due to dispersion. The ERT shows the combined processes, and ground truth from both changes in saturation (from tensiometers) and pore water electrical conductivity (measured in fluid from suction cups) captured the combined effects. This study also shows the valuable support of heterogeneous unsaturated zone modelling to explain the underlying processes.

Overall, there is a good correspondence between the estimated bulk resistivity calculated from Archie's law from a set of point measurements (combination of soil water sampling and measurements of soil suction) and the inversion of time-lapse cross-borehole ERT measurements of the same vertical profile. Hence, the study reveals that with some confidence, ground truthing data of either soil suction or conductivity of pore water can help estimate the other factor (saturation or solute concentration) when combined with time-lapse electrical resistivity measurements. Modelling of the same experiment in a heterogeneous unsaturated zone reveals that some variability of such measurements can be expected and must be included in the translation of changes in electrical resistivity to either saturation changes or plume movement. In this example, temperature effects have minimal influence on the interpretation of results.

Based on the results of this study, for such snowmelt induced contamination problems, a monitoring program for the unsaturated zone should include a combination of time-lapse ERT combined with a limited set of tensiometers (or soil water content sensors) at different depths to monitor the soil water status, and unsaturated heterogeneous simulations, to indicate the most likely migration (e.g., the travel time) of contaminants. Alternatively, soil water sampling could be used, although this is more costly, is prone to clogging due to biofilm growth and installation is limited to the upper few metres of the soil profile.

ACKNOWLEDGEMENTS

DATA AVAILABILITY STATEMENT

The data that support the findings of this study are available from the corresponding author upon reasonable request.

ORCID

Esther Bloem https://orcid.org/0000-0002-7226-6401
Nicolas Forquet https://orcid.org/0000-0003-1154-5498
Andrew Binley https://orcid.org/0000-0002-0938-9070
Helen K. French https://orcid.org/0000-0001-8845-4987

REFERENCES

Archie, G.E. (1942) The electrical resistivity log as an aid in determining some reservoir characteristics. *Transactions of the American Institute of Mining, Metallurgical, and Petroleum Engineers*, 146, 54–62.

Binley, A. (2015) Tools and techniques: DC electrical methods. In: G. Schubert (Ed.) *Treatise on Geophysics*, 2nd edition. Burlington: Elsevier, Vol. 11, pp. 233–259, https://doi.org/10.1016/B978-0-444-53802-4.00192-5

Binley, A., Hubbard, S. S., Huisman, J. A., Revil, A., Robinson, D. A., Singha, K. *et al.* (2015) The emergence of hydrogeophysics for improved understanding of subsurface processes over multiple scales. *Water Resource Research*, 51, 3837–3866. https://doi.org/10.1002/2015WR017016

Cassiani, G., Bruno, V., Villa, A., Fusi, N. and Binley, A. (2006) A saline trace test monitored via time-lapse surface electrical resistivity tomography. *Journal of Geophysics*, 59(3), 244–259.

Chambers, J.E., Gunn, D.A., Wilkinson, P.B., Meldrum, P.I., Haslam, E., Holyoake, S. *et al.* (2014). 4D electrical resistivity tomography monitoring of soil moisture dynamics in an operational railway embankment. *Near Surface Geophysics*, 12, 61–72.

Feng, S. and Sen, N.P. (1985) Geometrical model of conductive and dielectric properties of partially saturated rocks. *Journal of Applied Physics*, 58, 3226–3243.

Forquet, N. (2009) *Two-phase flow modelling of vertical flow filters for wastewater treatment*. PhD thesis, University of Strasbourg, France.

French, H.K., Swensen, B., Englund, J.-O., Meyer, K.-F. and van der Zee, S.E.A.T.M. (1994). A lysimeter trench for reactive pollutant transport studies. In: Soveri, J. and Suokko, T. (eds.) *Future Groundwater Resources at Risk. International Association of Hydrogeological Science (IAHS), 13–16 June*. Helsinki: Finland IAHS Publication. Vol. 222, pp. 131–138.

French, H.K. and Van der Zee, S.E.A.T.M (1999) Field scale observations of small scale spatial variability of snowmelt drainage and infiltration, *Nordic Hydrology*, 30, 166–176.

French, H.K., Van der Zee, S.E.A.T.M. and Leijnse, A. (2001). Transport and degradation of propyleneglycol and potassium acetate in the unsaturated zone. *Journal of Contaminant Hydrology*, 49, 23–48.

French, H.K., Hardbattle, C., Binley, A., Winship, P. and Jakobsen, L. (2002) Monitoring snowmelt induced unsaturated flow and transport using electrical resistivity tomography. *Journal of Hydrology*, 267, 273–284.

French, H.K. and Binley, A. (2004) Snowmelt infiltration: monitoring temporal and spatial variability using time-lapse electrical resistivity. *Journal of Hydrology*, 297(1–4), 174–186.

Geuzaine, C. and Remacle, J.-F. (2009) Gmsh: a three-dimensional finite element mesh generator with built-in pre- and post-processing facilities. *International Journal for Numerical Methods in Engineering*, 79, 1309–1331.

Hayley, K., Bentley, L., Gharibi, M. and Nightingale, M. (2007). Low temperature dependence of electrical resistivity: Implications for near surface geophysical monitoring. *Geophysical Research Letters*, 34, 18. https://doi.org/10.1029/2007GL031124.

Hubbard, S.S. and Rubin Y. (2000) Hydrogeological parameter estimation using geophysical data: a review of selected techniques. *Journal of Contaminant Hydrology*, 45, 3–34

Jørgensen, P. and Østmo, S.R. (1990). Hydrogeology in the Romerike area, southern Norway. *NGU Bulletins*, 418, 19–26

Kemna, A., Binley, A., Day-Lewis, F., Englert, A., Tezkan, B., Vanderborght, J. *et al.* (2006) Solute transport processes. In: Vereecken H., Binley, A., Cassiani, G., Revil, A., and Titov, K. *Applied Hydrogeophysics. NATO Science Series, IV: Earth and Environmental Sciences*. Dordrecht: Springer, Vol. 71, pp. 117–160.

Köestel, J., Kemna, A., Javaux, M., Binley, A. and Vereecken, H. (2008) Quantitative imaging of solute transport in an unsaturated and undisturbed soil monolith with 3D ERT and TDR. *Water Resources Research*, 44, W12411. https://doi.org/10.1029/2007WR006755.

Krautblatter, M., Verleysdonk, S., Flores-Orozco, A. and Kemna, A. (2010) Temperature-calibrated imaging of seasonal changes in permafrost rock walls by quantitative electrical resistivity tomography (Zugspitze, German/Austrian Alps). *Journal of Geophysical Research*, 115(F2), 1–15.

Lesmes, D.P. and Friedman, S.P. (2005) Relationships the electrical and hydrogeological properties of rocks and soils. In: Rubin, Y. and Hubbard S.S. (Eds.) *Hydrogeophysics*. Dordrecht: Springer, pp. 87–128.

Llera, F.J., Sato, M., Nakatsuka, K. and Yokoyama, H. (1990). Temperature dependence of the electrical resistivity of water-saturated rocks. *Geophysics*, 55(5), 576–585. https://doi.org/10.1190/1.1442869.

Miller, E.E. and Miller, R. D. (1956). Physical theory for capillary flow phenomena. *Journal of Applied Physics*, 27, 324–332.

Mualem, Y. and Friedman, S.P. (1991) Theoretical prediction of electrical conductivity in saturated and unsaturated soil. *Water Resource Research*, 27, 2771–2777.

Pedersen, T.S. (1994) *Væsketransport i Umettet sone, stratigrafisk beskrivelse av toppsedimentene på forskningsfeltet, Moreppen, og bestemmelse av tilh¢rede hydrauliske parametre* [Flow in the unsaturated zone, stratigraphic description of the top sediments at the research station, Moreppen, and the determination of hydraulic parameters]. M.Sc. thesis, Department of Geology, University of Oslo, pp. 1–122

Rein, A., Hoffmann, R., and Dietrich, P. (2004). Influence of natural time-dependent variations of electrical conductivity on DC resistivity measurements. *Journal of Hydrology*, 285, 215–232. https://doi.org/10.1016/j.jhydrol.2003.08.015.

Šimůnek, J., van Genuchten, M. Th. and Šejna, M. (2016) Recent developments and applications of the HYDRUS computer software packages. *Vadose Zone Journal*, 15(7), 25. https://doi.org/10.2136/vzj2016.04.0033.

Tuttle, K.J. (1997) *Sedimentological and hydrogeological characterisation of a raised ice-contact delta— the Preboreal delta-complex at Gardermoen, southeastern Norway*. PhD thesis, Department of Geology, University of Oslo.

Tso, C.-H.M., Kuras, O., Wilkinson, P.B., Uhlemann, S., Chambers, J.E., Meldrum, P.I. *et al.* (2017) Improved characterisation and modelling of measurement errors in electrical resistivity tomography (ERT) surveys. *Journal of Applied Geophysics*, 146, 103–119.

Uhlemann, S., Chambers, J., Wilkinson, P., Maurer, H., Merritt, A., Meldrum, P. *et al.* (2017) Four-dimensional imaging of moisture dynamics during landslide reactivation. *Journal of Geophysical Research: Earth Surface*, 122(1), 398–418.

Van Genuchten, M. Th. (1980) A closed form equation for predicting the hydraulic conductivity in soils. *Soil Science Society of America Journal*, 44, 892–898.

Vereecken H., Binley, A., Cassiani, G., Revil, A., and Titov, K. 2006 *Applied Hydrogeophysics*. Nato Science Series: IV: Earth and Environmental Science, Vol. 71, Dordrecht: Springer, 383 pp.

Winship, P., Binley, A. and Gomez, D. (2006) Flow and transport in the unsaturated Sherwood Sandstone: characterization using cross-borehole geophysical methods. *Geological Society, London, Special Publications*, 263, 219–231. https://doi.org/10.1144/GSL.SP.2006.263.01.12.

Wu, Y., Nakagawa, S., Kneafsey, T.J., Dafflon, B., and Hubbard, S. (2017) Electrical and seismic response of saline permafrost soil during freeze–thaw transition. *Journal of Applied Geophysics*, 146, 16–26. https://doi.org/10.1016/j.jappgeo.2017.08.008.